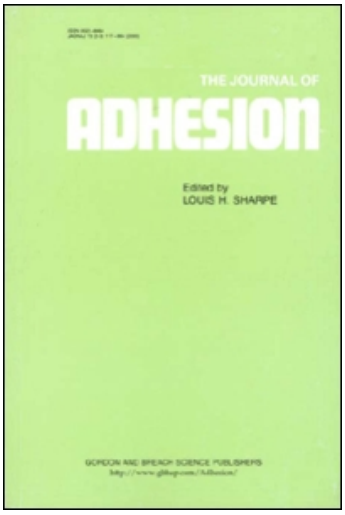

The Journal of Adhesion
Publication details, including instructions for authors and subscription information:
http://www.informaworld.com/smpp/title~content=t713453635

Influence of Layer Thickness on Cohesive Properties of an Epoxy-Based Adhesive—An Experimental Study

Thomas Carlberger[a]; Ulf Stigh[b]
[a] SAAB Automobile AB, Trollhättan, Sweden [b] University of Skövde, Skövde, Sweden

Online publication date: 04 August 2010

To cite this Article Carlberger, Thomas and Stigh, Ulf(2010) 'Influence of Layer Thickness on Cohesive Properties of an Epoxy-Based Adhesive—An Experimental Study', The Journal of Adhesion, 86: 8, 816 — 835
To link to this Article: DOI: 10.1080/00218464.2010.498718
URL: http://dx.doi.org/10.1080/00218464.2010.498718

The Journal of Adhesion, 86:816–835, 2010

ISSN: 0021-8464 print/1545-5823 online
DOI: 10.1080/00218464.2010.498718

Taylor & Francis
Taylor & Francis Group

Influence of Layer Thickness on Cohesive Properties of an Epoxy-Based Adhesive—An Experimental Study

Thomas Carlberger[1] and Ulf Stigh[2]
[1]SAAB Automobile AB, Trollhättan, Sweden
[2]University of Skövde, Skövde, Sweden

Cohesive laws are determined for different layer thicknesses of an engineering adhesive. The shape of the cohesive law depends on the adhesive layer thickness. Of the two parameters of the cohesive law—the fracture energy and the strength—the fracture energy is more sensitive to thickness variation than the strength. The fracture energy in peel mode (Mode I) increases monotonically as the thickness is increased from 0.1 to about 1.0 mm. At an adhesive thickness of 1.5 mm, the fracture energy is slightly lower than for a 1.0 mm adhesive thickness, indicating a maximum between 1.0 and 1.5 mm. In shear mode (Mode II), the thickness dependence is not as strong, but an increasing trend in fracture energy with increasing adhesive thickness is evident. A slight decrease in strength with increasing adhesive thickness is found in both loading modes.

Keywords: Adhesive joining; Cohesive zone model; Experimental; Fracture; Thickness dependence

NOMENCLATURE

a	Initial crack length
b	Specimen width
Ø	Diameter
ε, γ	Peel strain, shear strain
$\dot{\varepsilon}$, $\dot{\gamma}$	Strain rate (peel, shear)
F	Force
δ	Deflection at loading point
E	Young's modulus

Received 18 November 2009; in final form 18 March 2010.
Address correspondence to Thomas Carlberger, SAAB Automobile AB, SE-461 80, Trollhättan, Sweden. E-mail: thomas.carlberger@gm.com

h	Adhesive layer thickness
H	Adherend height
I	Moment of inertia
J	Energy release rate
J_c	Critical energy release rate, fracture energy
k	Initial stiffness
K_{IC}	Fracture toughness in Mode I
L	Specimen length
$\mathbf{n}$	Normal vector
σ, $\hat{\sigma}$	Peel stress, strength in Mode I
S	Integration path
τ, $\hat{\tau}$	Shear stress, strength in Mode II
$\mathbf{T}$	Traction vector
θ	Rotation of the adherend at the loading point
$\mathbf{u}$	Displacement vector
ν	Shear deformation at adhesive tip
W	Strain energy density
w	Peel deformation at adhesive tip
x	Length coordinate starting at adhesive tip

1. INTRODUCTION

Emission of carbon dioxide is driving the automotive industry to find methods of reducing fuel consumption. An efficient way to do this is to reduce the weight of the vehicle; the car body structure accounts for approximately one fifth of the total vehicle weight. This can be minimized by the use of multi-material structures, leading to a joining challenge. In the car industry, spot welding is the traditional joining technique for mono-material joining. That is, to join steel to steel or to join aluminium to aluminium, etc. Although this method has many advantages, it is essentially limited to mono-material joints. Adhesive joining is a well-established joining technique in many industrial areas, but in the car industry, until recently, this technique has almost exclusively been used in load bearing structures for extreme carbon fibre-reinforced race cars. Recent development of adhesive joining techniques has enabled mass production of adhesively bonded car body structures. With adhesive joining, similar or dissimilar materials may not only be joined, improvements of both stiffness and strength are achieved simultaneously compared with discrete joining methods, such as spot welding or riveting, *cf., e.g.*, [1–3]. The main reason for the increased stiffness is that for adhesively joined structures, the adherends are prevented from deforming, as opposed to the case with deforming between the discrete fasteners, which are spaced at a

certain distance. The increased strength is possible due to the high strength of crash-toughened adhesives and the relatively larger joining area inherent with the adhesive joining method.

During product development, computer simulations are required to give reliable information for the engineers. Efforts are made to reduce testing to a minimum due to the slow and expensive process of manufacturing test objects and evaluating tests. The testing performed today is mainly done to fulfil legal requirements and requirements from independent organisations as, *e.g.*, European New Car Assessment Programme (Euro NCAP). Computer simulations are much more time and cost efficient, on the essential condition that the simulations are reliable. Crash simulation is done by use of the explicit FE-method, *cf.*, *e.g.*, [4]. A possibility for modelling adhesives with finite elements is given by the cohesive zone modelling technique and the adhesive layer theory, according to which the deformation of the adhesive layer is dominated by deformation Mode I (peel) and deformation Modes II and III (shear) *cf.*, *e.g.*, [5]. The parameters of the cohesive zone model are determined by performing physical tests. In [6], an experimental method for determining the cohesive zone properties for the adhesive based on equilibrium of energetic forces and the adhesive layer theory is presented. The method is shown to be capable of predicting the strength of the adhesive with good (engineering) precision. Determining material parameters and validating simulation models is essential to the reliability of this methodology, *cf.*, *e.g.*, [7]. Cohesive parameters, 1: strength (peak stress) and 2: fracture energy (area under cohesive law), for different modes of deformation and for the nominal adhesive thickness 0.2 mm are measured and determined in [8,9]. The difficulty of obtaining a fixed adhesive thickness, *e.g.*, in a car body structure, gives rise to the demand of understanding how the adhesive thickness influences joint strength. During the manufacturing process, a car body structure is assembled and subsequently painted. During the paint curing in the paint oven, the adhesive is also cured. Prior to curing, the adhesive has very limited strength. To secure the car body integrity before curing, some means of additional joining must be provided. This may be riveting or bolting for multi-material joints; for mono-material joints, spot welding is often used. The car body structure is built up by joining large preformed parts mostly consisting of sheet metal. Manufacturing tolerances give rise to uneven gap width that should be taken up by the adhesive. The mechanical joints will keep the parts firmly together but will allow the gap width to vary between the fasteners. Thus, it is essential to understand how the strength of adhesive joints varies with the thickness of the adhesive layer.

A literature review shows that studies of thickness dependence of adhesives have been limited to either the variation of fracture energy with adhesive thickness, the strength, or both. No complete cohesive laws have been studied for this effect. In [10], the authors studied the fracture energy of an epoxy adhesive and found that the fracture energy increases for increasing adhesive thickness until a maximum is reached at about 0.5- to 1.0-mm thickness, followed by a decline in fracture energy to a level insensitive to further increase of the adhesive thickness. This level corresponds to the bulk fracture energy of the adhesive. In a study of the fracture energy in Mode I of a ductile adhesive it is found that the fracture toughness shows a maximum for an adhesive thickness of about 0.2 mm [11]. In [12], an increasing fracture energy in Mode I for thickness 0.1 to 0.7 mm is noted for a brittle adhesive, while, for a ductile adhesive, the fracture energy in Mode I shows a minimum at approximately 30 μm with increasing fracture energy for thicker and thinner adhesive thickness between 2.5 and 75 μm. Both the strength and the fracture energy are used in [13] to analyse the influence of the bond line thickness in Modes I and II. The author finds a decreasing strength with increasing adhesive thickness, but increasing fracture energy for adhesive thicknesses below a threshold value, about 1 mm, above which the fracture energy assumes the bulk adhesive fracture energy regardless of further thickness increase. In [14] the DCB specimen is used to show how the fracture energy varies with bond line thickness in Mode I. They also review the literature on the typical thickness dependence for different types of adhesives. In [15] the napkin ring specimen and the ENF-specimen are used for analysing both a brittle and a ductile epoxy adhesive in Mode II. The ductile adhesive showed increasing fracture energy for increasing adhesive thickness up to 0.6 mm. The brittle adhesive showed an increase of fracture energy with increasing adhesive thickness until a plateau was reached at about 20 μm thickness and extended to about 60 μm, whereafter a decline in fracture energy was observed. The author ascribes this phenomenon to the increase in volume available for developing plastic deformation. The plateau and decline of the fracture energy are explained by the proposition that the plastic deformation at the crack tip no longer occupies the entire bond thickness, but instead it concentrates around the crack tip adjacent to the interface layer close to the adherend. In [16] the same increase of Mode II fracture energy with increasing adhesive thickness is found using the compact pure shear specimen and a rubber modified epoxy adhesive. In [17], the influence on the fracture toughness by thickness variation is explained by studying how the extent of the plastic zone influences the J-integral. In a study, mainly

using the wedge-peel test, it is found that the fracture energy of the adhesive can be divided into two parts, Γ_0 and Γ_p, where Γ_0 is the intrinsic work of fracture associated with the embedded cohesive zone response and Γ_p is the contribution arising from plastic dissipation and stored elastic energy within the adhesive layer [18]. The plastic contribution, Γ_p, increases with increasing bond line thickness in the fully plastic regime and then decreases to reach a constant value for very thick adhesive layers.

A promising method, when performing simulation of adhesive joints, is the use of cohesive finite elements, *cf. e.g.*, [19]. The cohesive element presented in [20] is an element for efficient modelling and simulation of adhesive joints between shell elements. This special element uses a cohesive zone model for determining the response on the connected shell elements. The fracture energy is known to change with the adhesive thickness, *cf., e.g.*, [21–26]. Thus, the influence of thickness on the parameters of the cohesive zone model must be determined. The scope of the work described in this paper is to determine the thickness influence on the cohesive model, also termed cohesive law, for an epoxy-based structural adhesive.

In [21], a simple peel test for flexible substrates is used together with the T-peel test for rubbery adhesives of thickness between 0.2 and 6 mm. It is shown that the fracture energy increases with increasing adhesive thickness until the thickness reaches 1 mm for a polyethylene terephthalate adhesive. For values above 1 mm, the fracture energy is not affected by the increase in thickness. In [14], the thickness influence on fracture energy in Mode I is studied for toughened adhesives. The author finds increasing fracture energy up to a certain adhesive thickness and, thereafter, a decrease to a slightly lower value, independent of any further increase in thickness. The author ascribes these findings to the existence of a plastic zone ahead of the crack tip and the constraint upon this zone by the stiffer adherends. In [22], shear experiments are reported using the napkin ring specimen and the end-notched flexure (ENF) specimen with a toughened epoxy-based adhesive. The author finds a logarithmically increasing ultimate shear strain with decreasing bond thickness and a monotonically increasing normalised Mode II fracture energy with decreasing bond thickness below a certain threshold thickness value. Above this threshold value, the Mode II fracture energy is insensitive to bond thickness. In [23], experiments and numerical studies of effects of the bond thickness performed using the compact tension specimen are presented. The authors find the maximum fracture toughness for the bond thickness to be 0.8 mm. The reason for this, they report, is that the crack tip stress field is affected by the adhesive thickness through the restriction of plastic

deformation such that the crack tip stress field is "flattened" by the adherends and extended along the bond line. In [24], a double cantilever beam (DCB) specimen is used to determine the effects of bond line thickness on the fracture energy for a rubber-modified epoxy adhesive. The authors find a linearly increasing fracture energy with increasing adhesive thickness extending to a maximum value, followed by a rapid asymptotic decline towards a value representing the toughness of bulk adhesive material. The adhesive thickness, for which the maximum J_c occurs, is shown to be slightly less than 1 mm. In [25], a lap shear joint with an L-shaped profile to stiffen the joint is tested for three different adhesive thicknesses. Adherends are manufactured from glass-fibre-reinforced vinyl-ester composite laminates using resin infusion and bonded with an epoxy adhesive. The fracture load decreases monotonically with increasing adhesive thickness. The lap-shear test generally produces a mixed mode stress field, and in this case, with the stiffener un-symmetrically placed, the stress field is non-trivial. In a recent study [26], a modified Arcan fixture is used to find that the adhesive bond line thickness reduces the yield stress and failure strain, strongly in tensile loading and moderately in mixed mode and shear mode.

In the present work, the complete cohesive law is determined for Modes I and II for varying adhesive thicknesses, with J_c equal to the area under the cohesive law. The specimens used are the DCB and ENF specimens for Modes I and II, respectively. The material in the adherends in both the DCB and ENF specimens is Rigor Uddeholm tool steel[1] with a minimum yield-strength of 500 MPa. With the chosen specimen geometries, this ensures elastic behaviour of the adherends throughout the experiments. The adhesive is an epoxy-based structural adhesive commonly used in the automotive industry: Dow Betamate® XW1044-3.[2]

2. THEORETICAL BACKGROUND AND DESIGN OF EXPERIMENTS

The deformation modes for the adhesive joint are shown in Fig. 1. It is assumed that the adhesive layer is thin and flexible compared with the adherends. With metal adherends, Young's modulus of epoxy adhesives is typically less than 5% of that of the adherends. For a nominal adhesive thickness, $h = 0.2$ mm, the cohesive laws in peel (Mode I), $\sigma(w)$, and in shear (Modes II and II), $\tau(v)$, for the adhesive are presented in Fig. 2. In the present work, the DCB specimen, *cf.*, Fig. 3, is used for

[1]UDDEHOLM SVENSKA AB, Mölndal, Sweden.
[2]Dow Automotive, Auburn Hills, MI, USA.

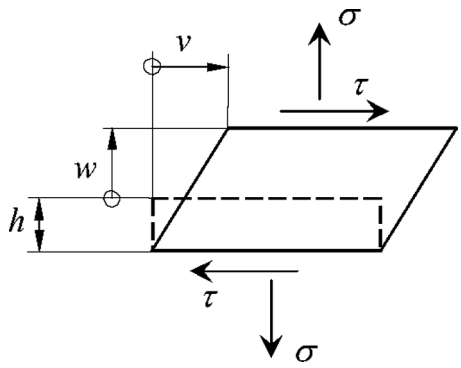

FIGURE 1 Deformation modes of the adhesive layer with thickness h: peel, w, and shear, v. Conjugated stress components σ and τ.

pure peel deformation. In [27] an exact inverse method for pure peel using the DCB specimen is developed. For pure shear an inverse method using the ENF specimen is developed, *cf.*, Fig. 4 and [28]. The inverse formulas are based on the use of alternative integration paths for the evaluation of the J-integral

$$J = \int_S (Wn_x - T_i u_{i,x}) \mathrm{d}S. \tag{1}$$

Here, the counter-clockwise integration path, S, can be chosen freely if the strain energy density, W, is independent of any explicit dependence of the x-coordinate, *cf.*, [29]. The outer unit normal to S is denoted $\mathbf{n}$ and

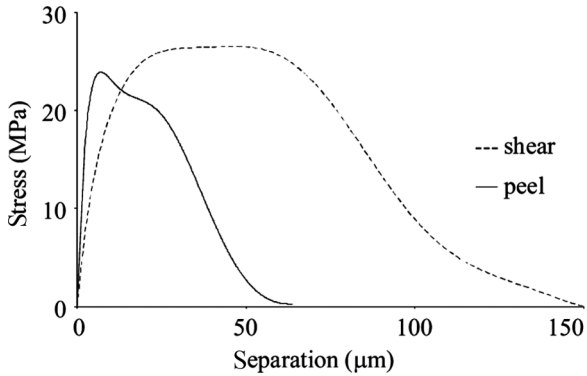

FIGURE 2 Cohesive laws in peel and shear for the engineering adhesive DOW Betamate® XW1044-3 with a 0.2-mm layer thickness.

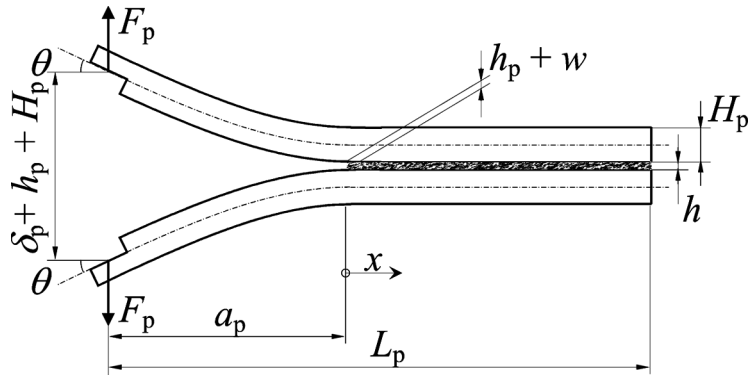

FIGURE 3 Double cantilever beam (DCB) specimen. The unbonded part of the specimen can be considered as a crack. That is, a_p is the crack length ($a_p = 80\,\text{mm}$). Adherend width, $b_p = 5\,\text{mm}$, adherend height, $H_p = 6.6\,\text{mm}$, specimen length, $L_p = 160\,\text{mm}$, adhesive thickness, h_p. Deformation is exaggerated for clarity.

the traction vector and displacement vectors are denoted **T** and **u**, respectively. Index notation is used with partial differentiation denoted by a comma and summation indicated by repeated indexes. Taking an integration path encircling the start of the adhesive layer gives

$$J = \int \sigma \mathrm{d}w + \int \tau \mathrm{d}v \tag{2}$$

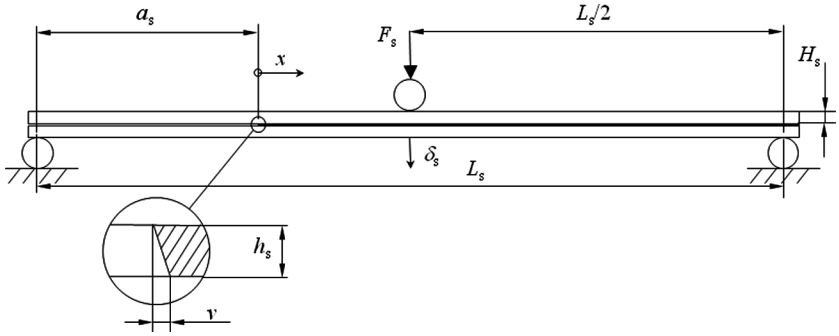

FIGURE 4 ENF specimen. Unbonded length, $a_s = 300\,\text{mm}$, length between supports, $L_s = 1000\,\text{mm}$, adherend height, $H_s = 16\,\text{mm}$, adherend width, $b_s = 32.8\,\text{mm}$, and adhesive thickness, h_s.

for peel and shear deformation. These relations show that cohesive laws are closely related to fracture mechanics. At the end of a fracture process, the cohesive stress, σ and τ, are zero, indicating that a crack has formed. After this moment, Eq. (2) shows constant J. Thus, the maximum value of J is identified with the fracture energy, J_c. That is, J_c equals the area under the cohesive law.

Now, taking an alternative integration path at the exterior boundary of the specimens give

$$J = \frac{2F_p\theta}{b_p}, \quad J = \frac{9F_s^2a_s^2}{16E_sb_s^2H_s^3} + \frac{3F_sv}{8b_sH_s} \tag{3a,b}$$

for the DCB- and ENF-specimens, respectively. Subscripts p and s indicate variables connected to peel (DCB) and shear (ENF) experiments, respectively. The geometries of the specimens are given by the height of the adherends, H, the width, b, and the crack length, a. Young's modulus for the adherends is denoted E and only enters Eq. (3b). During a peel experiment (DCB), the applied force, F, and the rotation of the loading point, θ, are measured as functions of the elongation, w, of the adhesive at the tip of the adhesive layer. During a shear experiment (ENF), the applied force, F, is measured together with the shear deformation, v, at the tip of the adhesive layer. By making the alternative expressions for J equivalent, the evolution of J with the deformation of the adhesive layer is derived from the measurements. Differentiation with respect to deformation, w or v, gives the cohesive law, *cf.*, Eq. (2). However, differentiation of experimental data elevates errors in the measured data. A useful method is to start with a least square adaption of a Prony-series to the J-data. Inspection of the success of the adaption to each experiment determines the number of terms to use in the Prony-series. Finally, the Prony-series is differentiated to produce the cohesive law, *cf., e.g.*, [7].

Equation (3b) is based on assuming linear elastic behaviour of the adherends during the experiments. This has to be checked both in the design of the specimens and in the evaluation of the experiments. It might need to be stressed that the adhesive is not assumed linearly elastic. An alternative expression to Eq. (3a) based on linear fracture mechanics is given in [30].

$$J = \frac{F_p^2}{E_pI_pb_p}\left(\frac{3E_pI_p\delta_p}{2F_p}\right)^{2/3}, \tag{4}$$

where E_p is Young's modulus of the adherends, I_p is the adherend cross sectional moment of inertia, and δ_p is the displacement of the

loading points. In the derivation of this equation, the adhesive is assumed rigid. In [31], it is shown that Eqs. (3a) and (4) give almost identical results for the DCB specimen geometry with reasonable cohesive laws for the adhesive. The error in fracture energy in using Eq. (4) is typically less than 4%.

The inverse methods have recently proven successful in determining the cohesive zone parameters for adhesives, *cf., e.g.*, [8,9]. The cohesive laws presented in Fig. 2 are determined by differentiation of the J-separation relations given in Fig. 5. The critical fracture energy is the energy released when the crack starts to propagate. In theory, with homogeneous adhesive properties this occurs when the derivative of J with respect to the adhesive deformation at the adhesive tip equals zero, *cf.*, Eq. (2). Although theoretically simple, this method to measure J_c for an adhesive may encounter practical problems. In some experiments, no horizontal asymptote is found in the J-curves. A straightforward method to identify the fracture energy is to observe the crack tip region and determine the moment of crack propagation visually. However, the fracture process of engineering adhesives involves nucleation, growth, and coalescing of many micro cracks. That is, it is virtually impossible to visually identify the moment of crack propagation by this method, *cf.*, *e.g.*, [9]. An alternative method used in this paper is described in the Appendix.

The initial crack length is created by a PTFE-film that also serves to control the adhesive layer thickness. Prior to applying the adhesive, the adherends are thoroughly cleaned with heptane and acetone. The

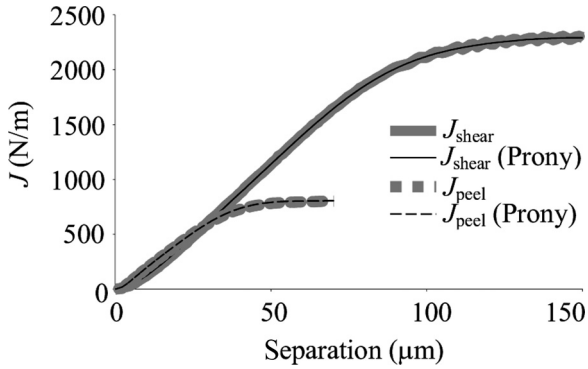

FIGURE 5 J – deformation relation. Epoxy adhesive DOW Betamate® XW1044-3 at $T = 20°C$, adhesive thickness 0.2 mm, $\dot{\varepsilon} = 1.7 \cdot 10^{-3}\,s^{-1}$ (peel) and $\dot{\gamma} = 5.0 \cdot 10^{-3}\,s^{-1}$ (shear).

curing of the adhesive is conducted at 180°C for 30 minutes, corresponding to the curing process for paint in automotive manufacturing. At room temperature, the uncured adhesive has a viscosity of 4 kPas. The DCB specimens are manufactured from plates of the adherend material. The plates are bonded with the PTFE-film at the initial crack location and at the end of the adhesive layer to ensure correct layer thickness. Subsequently, the plates are clamped together and cured in the curing oven following the manufacturer's specifications. After curing, slow cooling is allowed in order to minimise the influence of residual stresses. Next, the clamps are removed and the DCB plates are cut into specimens with a band saw. Finally, the DCB specimens are machined to specified width. The ENF specimens are bonded individually from prismatic tool steel bars separated by PTFE-film creating the initial crack and securing the correct adhesive layer thickness. The single added process in the manufacturing of the ENF specimens is a removal of excess adhesive after curing. The geometries for the DCB-specimens are given by $a_p = 80$ mm, $b_p = 5$ mm, $H_p = 6.6$ mm, and $L_p = 160$ mm, and for the ENF-specimens by $a_s = 300$ mm, $L_s = 1000$ mm, $H_s = 16$ mm, and $b_s = 32.8$ mm. The following nominal adhesive layer thicknesses are considered: $h_p = 0.1$, 0.2, 0.4, 0.6, 0.8, 1.0, and 1.6 mm (DCB) and $h_s = 0.1$, 0.2, 0.4, 0.6, 0.8, and 1.0 mm (ENF). The thickness is measured individually with a micrometer for each specimen.

3. TEST SETUP

3.1. DCB Experiments

A specially designed test machine is used for the testing of DCB-specimens, *cf.*, Fig. 6. The DCB specimen is oriented vertically in the centre of the machine. Both crossheads move symmetrically around the centre of the machine. Two horizontally working ball screws powered by an electric motor control the displacement, δ_p. A load cell measures the force, F_p. The rotation, θ, at the loading point is measured with an incremental shaft encoder. The position of the crossheads is measured with a linear potentiometer. Two linear variable differential transducers (LVDT) are in contact with the outside of the adherends to measure the elongation of the adhesive layer at the tip of the adhesive layer (not shown in Fig. 6). The crosshead speed, 1.8 mm/min (30 μm/s), is constant during an experiment and chosen such that no effects of inertia will affect the results. The test is quasi-static.

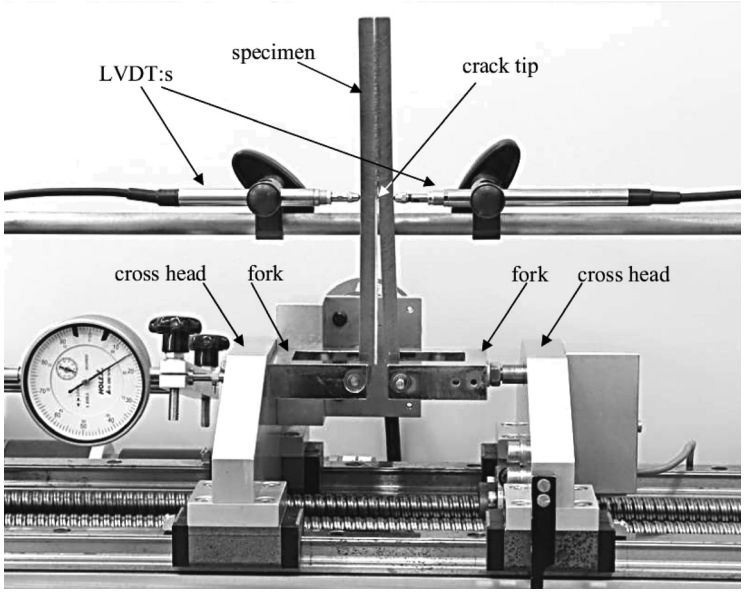

FIGURE 6 DCB test machine with LVDT's and specimen.

3.2. ENF Experiments

The ENF experiments are performed using a tensile test machine LLOYD LR10k plus,[3] *cf.*, Fig. 7. The supports are solid Ø 20-mm cylinders placed on stiff I-beams at ± 500 mm distance symmetrically from the machine centre line. The measurement of the adhesive tip deformation is done by an LVDT fixed to the adherends by a mechanical attachment (not shown in Fig. 7). The force, F_s, is measured with a load cell mounted on the crosshead, and the displacement, δ_s, is given by the crosshead position.

4. EXPERIMENTAL RESULTS

4.1. DCB Experiments

Cohesive laws in peel mode are determined for layer thicknesses between 0.1 and 1.6 mm, *cf.*, Fig. 8. Each cohesive law in Fig. 8a is averaged from five to eight specimens of a specific adhesive layer thickness. For statistical comparison, Fig. 8b shows the cohesive law

[3]Lloyd Instruments Ltd., West Sussex, UK.

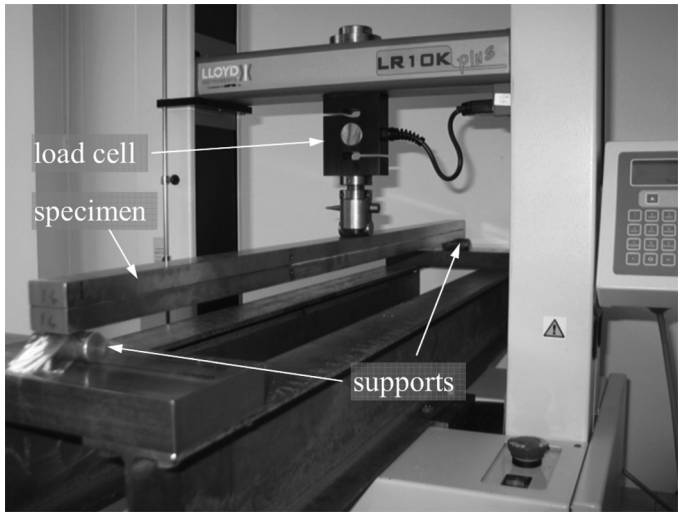

FIGURE 7 Tensile testing machine used for ENF experiments. An ENF specimen is mounted in the machine.

for each of the eight individual specimens for the adhesive thickness 0.8 mm and their average. The variation between each specimen is believed to be caused by strength variations along the adhesive bond line. The major thickness dependence is the decreasing steepness of the slope after the peak stress is passed. A wider peak region and larger critical separation are also observed as the layer thickness increases. These observations lead to an increase of the area under the cohesive law, which corresponds to an increase of the fracture energy, J_c. These results confirm the findings in [21,23,24] for the adhesive thicknesses between 0.2 and 1.6 mm, although in [21] a different type of adhesive is used.

Though the crosshead speed is constant, the strain rate varies during a DCB experiment, *cf.*, Fig. 9a. When the adhesive softens at the tip of the adhesive layer, the strain rate accelerates. Since the adhesive is polymer-based, and polymers are known to be strain rate dependent, it is plausible to expect a strain rate dependent cohesive law. The strain rate, at the moment the peak stress occurs, is relatively low, *cf.*, the triangle in Fig. 9a. The strain rate at the point when half the fracture energy is consumed is higher and may be considered as a more representative value of the strain rate over the duration of the experiment, *cf.*, the circle in Fig. 9a. Thus, the strain rate is measured in this way throughout the paper. The strain rate in each experiment is plotted against the adhesive thickness, h, in Fig. 9b.The

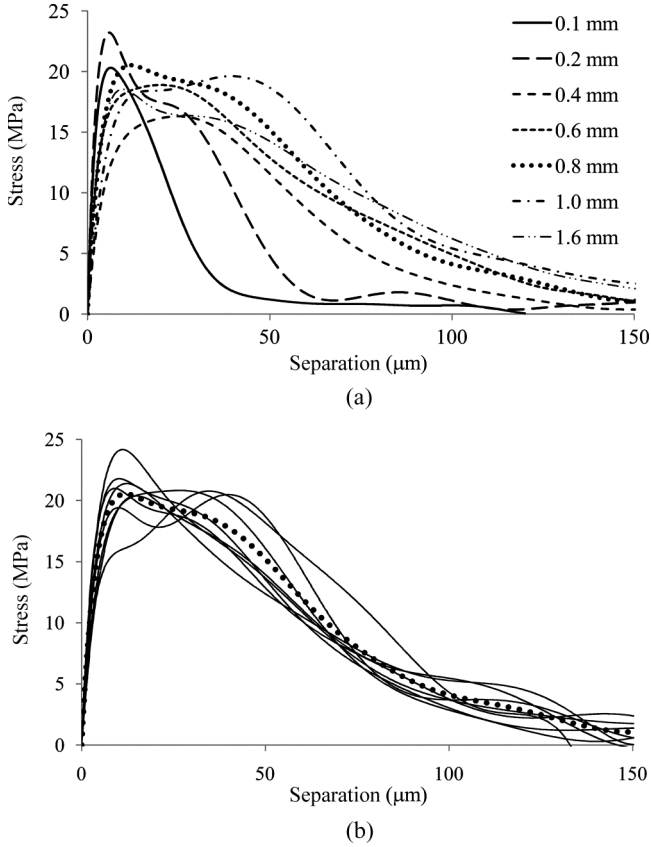

FIGURE 8 (a) Averaged cohesive laws for thicknesses 0.1–1.6 mm in peel mode. (b) Cohesive law for eight specimens (thin lines) at adhesive thickness 0.8 mm and the average (thick line).

crosshead speed is 1.8 mm/s (30 μm/s) for all thicknesses except for 0.2 mm, where it is 0.6 mm/min (10 μm/s). The strain rate measurement shows inverse thickness dependence. One significant difference is noticed at thickness 0.2 mm, which may be explained by the lower load rate. In [32], the strain rate dependence in peel is studied for the present adhesive. In the work performed for this paper, there is a slight strain rate dependence of both the fracture energy and the peak stress, but it does not change the results noticeably. This is likely to be the reason why, in Fig. 10, the fracture energy at $h = 0.2$ mm does not differ significantly from the overall trend. The results in Fig. 10a show increasing fracture energy with increasing adhesive thickness

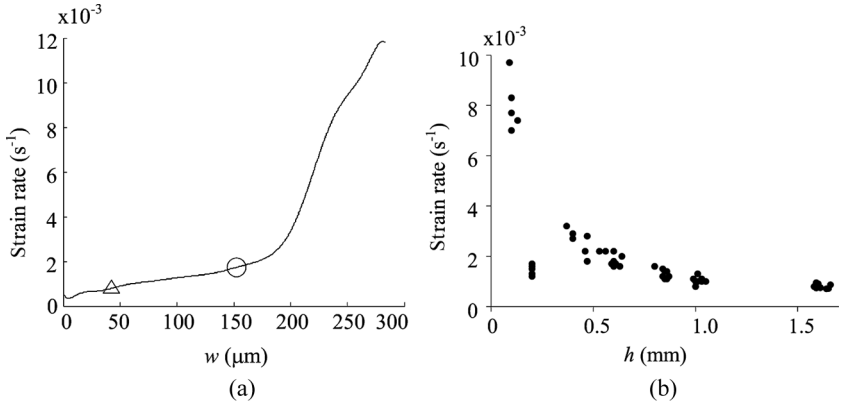

FIGURE 9 (a) Strain rate variation with the deformation, w, during one experiment. Triangle marks peak stress (strength), circle marks half the consumed fracture energy, J_c. (b) Strain rate variation with the thickness, h.

up to 1.0 mm, and at 1.6 mm slightly lower fracture energy. The fracture energy for adhesive thickness 0.1 mm fit in an extrapolated manner between 0.2 mm and zero thickness. Figure 10b shows strength *vs.* the adhesive thickness, h. As shown, the strength appears virtually independent of the layer thickness in peel (Modes I).

4.2. ENF Experiments

Cohesive laws in shear mode are determined for layer thicknesses between 0.1 and 1.0 mm, *cf.*, Fig 11. Each cohesive law in Fig. 11 is

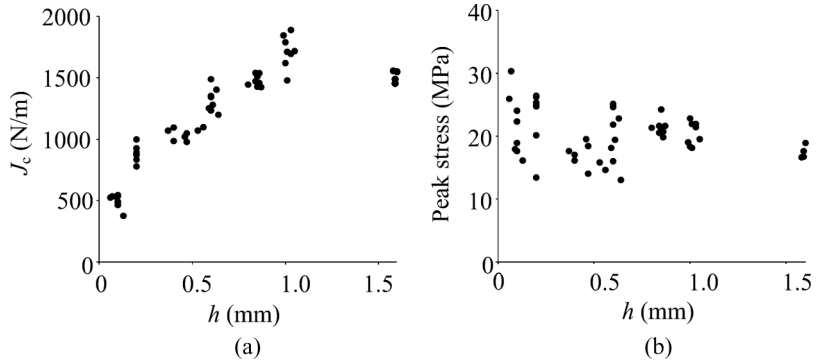

FIGURE 10 (a) Fracture energy and (b) strength *vs.* adhesive thickness, h, for peel mode.

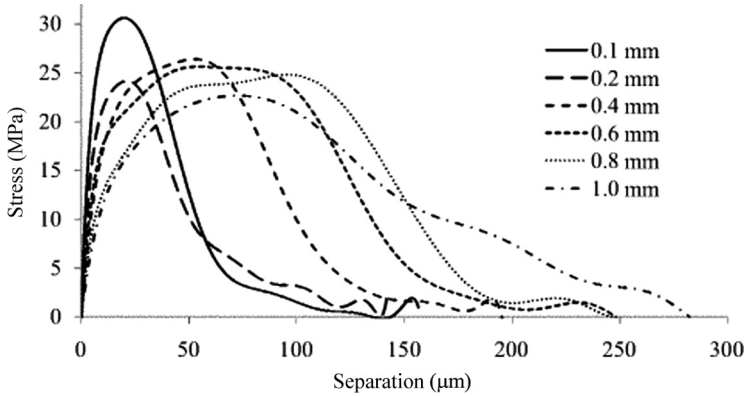

FIGURE 11 Cohesive laws for adhesive thicknesses 0.1–1.0 mm in shear mode.

averaged from two to three specimens at the actual layer thickness. The major thickness dependence is to increase the fracture energy, J_c, with increasing thickness. The strain rate varies also during an ENF experiment, *cf.*, Fig. 12a. When the adhesive softens at the tip of the adhesive layer, the strain rate accelerates. The strain rate in each experiment is plotted *vs.* the adhesive thickness, h, in Fig. 12b. The strain rate for the ENF experiments declines with increasing thickness in the same manner as for the DCB experiments, *cf.*, Fig. 12b. Fracture energy and strength are given in Fig. 13. The

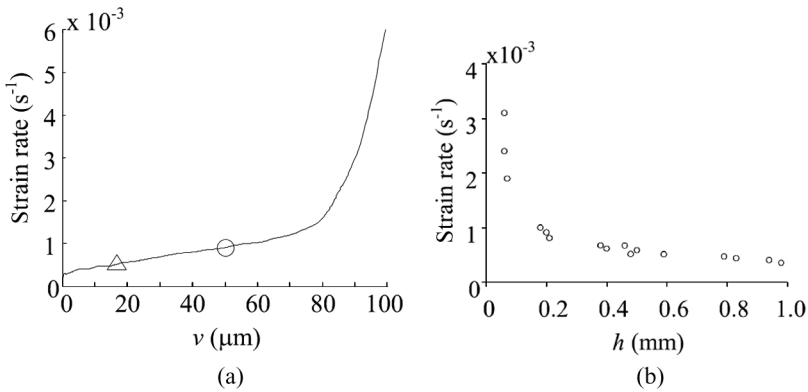

FIGURE 12 (a) Strain rate variation with deformation, v, during one experiment. Triangle marks peak stress, circle marks half the consumed fracture energy, J_c. (b) Strain rate variation with adhesive thickness, h.

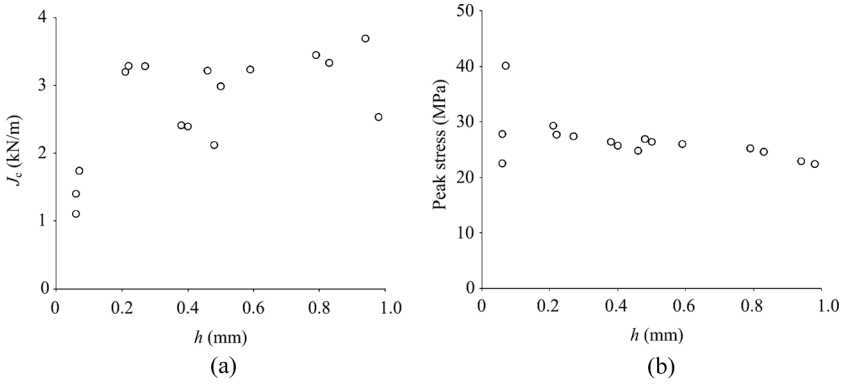

FIGURE 13 (a) Fracture energy and (b) strength *vs.* adhesive thickness, h, for shear mode.

fracture energy appears virtually unaffected by increases of the layer thickness above about 0.2 mm. The results for shear mode at the thickness 0.2 mm are taken from a different experiment, performed earlier using a different batch of the adhesive. The behaviour of the fracture energy in shear differs significantly from the findings in [22], although the adhesives are toughened epoxies in both studies. The strength appears to decrease slightly with increasing thickness. This is probably an effect of the decreasing strain rate with increasing thickness, *cf.*, [32].

5. CONCLUSIONS

The adhesive thickness influences the shape of the cohesive law and, thus, the fracture energy strongly. However, for both peel and shear mode, the strength shows little thickness dependence, although a slight decrease in strength with increasing adhesive thickness is indicated. The fracture energy in peel (Mode I) increases monotonically as the thickness is increased from 0.1 to about 1.0 mm. At 1.6 mm, the fracture energy is slightly lower than for 1.0 mm, indicating that the fracture energy has a maximum between 1.0 and 1.6 mm. These findings are in accordance with those of [14] where the influence of the relatively stiffer adherends on the size of the process zone is described as the mechanism responsible for the thickness dependence. Especially for toughened adhesives, which fracture by large plastic deformation, there are two mechanisms governing the thickness dependence of such adhesives. The plastically dissipated energy governs the fracture energy and is dependent on the length of the plastic zone. The (stiff)

adherends impose a restriction of the extent of the plastic zone, which decreases the fracture energy with decreasing adhesive thickness. A second effect will increase the peel stresses ahead of the crack tip. This effect increases the length of the plastic zone and for an adhesive thickness approximately equal to the diameter of the plastic zone for the bulk adhesive, the fracture energy reaches a maximum for the adhesive.

In shear mode, the thickness dependence is not as strong, but a similar trend is evident below about 0.2 mm. The larger scatter in the shear study makes the conclusions less clear, although trends are visible.

FUTURE WORK

The study shows the need for more experimental data to reduce uncertainties in the evaluation of the thickness dependence. More recently developed crash-resistant adhesives will be interesting to analyse. These are known to show much higher fracture energy while the peak stress is similar to that of the present adhesive.

ACKNOWLEDGMENTS

The author thanks the Swedish Consortium for Crashworthiness for funding this project. Special thanks are directed to Mr. Stefan Zomborcsevics for preparing specimens and Dr. Anders Biel for helping with the experiments.

REFERENCES

[1] Lee, M. M. K., Pine, T., and Jones, T. B., Automotive Box Section Design Under Torsion. Part 1: Finite Element Modeling Strategy. *Proc. Instn Mech. Engrs, Part D: J. Automobile Engineering* **214** (4), 347–360 (2000).
[2] Lee, M. M. K., Pine, T., and Jones, T. B., Automotive Box Section Design Under Torsion. Part 2: Behavior and Implications on Weight Reduction. *Proc. Instn. Mech. Engrs., Part D: J. Automobile Engineering* **214** (5), 473–485 (2000).
[3] Seeds, A. and Sheasby, P. G., Evaluation of adhesive joining systems in aluminum box beams, SAE technical paper 870152 (SAE, Warrendale, PA, 1987).
[4] Belytschko, T., Liu, W. K., and Moran, B., *Nonlinear Finite Elements for Continua and Structures*, (John Wiley and Sons, Chichester, 2000).
[5] Schmidt, P. and Edlund, U., *Int. J. Numer. Meth. Eng.* **66**, 1271–1308 (2006).
[6] Andersson, T. and Stigh, U., *Int. J. Solids Struct.* **41**, 413–434 (2004).
[7] DuBois, P. A., Crashworthiness Engineering, Course Notes. (Livermore Software Technology Corporation, Livermore, 2004).
[8] Leffler, K., Alfredsson, K. S., and Stigh, U., *Int. J. Solids Struct.* **44**, 530–545 (2007).
[9] Andersson, T. and Biel, A., *Int. J. Fract.* **141**, 227–246 (2006).

[10] Bascom, W. D. and Cottington, R. L., *Journal of Adhesion* **7** (4), 333–346 (1978).
[11] Chai, H., Bond Thickness Effect in Adhesive Joints and its Significance for Mode I Interlaminar Fracture of Composites, ASTM Special Technical Publication, 209–231 (1986).
[12] Chai, H., *Engineering Fracture Mechanics* **24** (3), 413–431 (1986).
[13] Kinloch, A. J., *Adhesion and Adhesives: Science and Technology*, (Chapman and Hall, London, 1987).
[14] Mall, S. and Ramamurthy, G., *International Journal of Adhesion and Adhesives* **9** (1), 33–37 (1989).
[15] Chai, H., *Int. J. Fracture* **60** (4), 311–326 (1993).
[16] Daghyani, H. R., Lin, Y., and Mai, Y.-W., *Journal of Adhesion* **56** (1–4), 171–186 (1996).
[17] Ikeda, T., Yamashita, A., Lee, D., and Miyazaki, N., *J. Engineering Materials and Technology, Transactions of the ASME* **122** (1), 80–85 (2000).
[18] Pardoen, T., Ferracin, T., Landis, C. M., and Delannay, F., *Journal of the Mechanics and Physics of Solids* **53** (9), 1951–1983 (2005).
[19] Reedy, E. D. and Mello, F. J., *J. Compos. Mat.* **31** (8), 812–831 (1997).
[20] Carlberger, T., Alfredsson, K. S., and Stigh, U., *Int. J. Comp. Meth. Eng. Sc. Mech.* **9** (5), 288–299 (2008).
[21] Dillard, D. A., Pocius, A. V., and Chaudhury, M., *Adhesion Science and Engineering*, (Elsevier, Amsterdam, 2002), Vol. 1, p. 806.
[22] Chai, H., *Int. J. Fract.* **130**, 497–515 (2004).
[23] Choi, J. Y., Kim, H. J., Lim, J. K., and Mai, Y.-W., *Key Engng. Mat.* 270–273, 1200–1205 (2004).
[24] Duan, K., Hu, X., and Mai, Y.-W., *J. Adhesion Sci. Technol.* **18** (1), 39–53 (2004).
[25] Taib, A. A., Boukhili, R., Achiou, S., Gordon, S., and Boukehili, H., *Int. J. Adhesion & Adhesives* **26**, 226–236 (2006).
[26] Davies, P., Sohier, L., Cognard, J.-Y., Bourmaud, A., Choqueuse, D., Rinnert, E., and Créac'hcadec, R., *Int. J. Adhesion Adhesives* **29**, 724–736 (2009).
[27] Olsson, P. and Stigh, U., *Int. J. Fract.* **41**, 71–76 (1989).
[28] Alfredsson, K. S., *Int. J. Solids Struct.* **41**, 4787–4807 (2004).
[29] Rice, J. R., *J. Applied Mech.* **33**, 379–385 (1968).
[30] Tamuzs, V., Tarasovs, S., and Vilks, U., *Compos. Sci. Technol.* **63**, 1423–1431 (2003).
[31] Biel, A. and Stigh, U., *Eng. Fract. Mech.* **75** (10), 2968–2983 (2008).
[32] Carlberger, T., Biel, A., and Stigh, U., *Int. J. Fract.* **155**, 155–166 (2009).
[33] Stigh, U., *International Journal of Fracture* **37**, R13–R18 (1988).

APPENDIX: DETERMINING THE FRACTURE ENERGY FROM EXPERIMENTS

Determining the fracture energy, J_c, from experiments is in theory easy. The critical fracture energy is obtained by reading the J-value at the point on the J-w curve where the tangent becomes horizontal corresponding to zero stress, *cf.* Eqs. (2) and (3). However, in some cases, we find that the J-curve has a slightly positive tangent. This may be explained by, *e.g.*, non-homogeneous properties along the adhesive, pre-damaged adhesive at the tip, or strain rate effects during loading. If the measured J-w curve does not have a zero

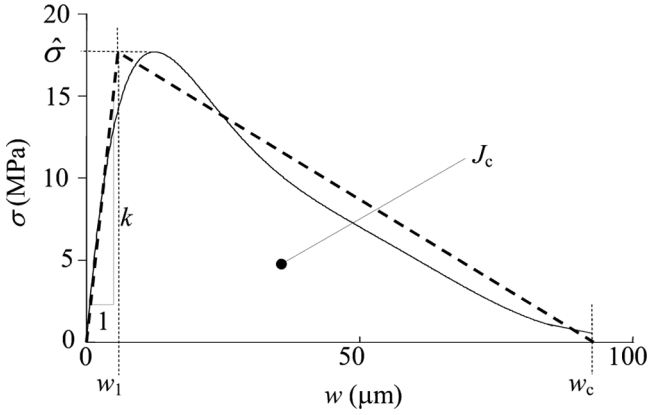

FIGURE A1 Solid curve: cohesive law obtained by differentiation of the J-w relation. Dotted curve: a saw tooth approximation.

tangent, a special method is used. A saw tooth approximation of the cohesive law is made by adapting the strength, $\hat{\sigma}, \hat{\tau}$, and the initial stiffness, k, to the experimental results. An approximate guess of the fracture energy, J_c, is made by choosing a value of w_c, *cf.* Fig. A1. Assuming that the saw tooth model is a good approximation of the cohesive law, a simulation of the F–δ relation is made using a closed form solution [33]. Now, if the simulated F–δ relation does not agree with the experimental data, the critical separation, w_c, is changed until the saw tooth model returns an F–δ relation in good agreement with the measured F–δ relation. This method is valid even if the saw tooth model is not a good approximation of the cohesive law since the F–δ relation is only slightly sensitive to the details of the cohesive law in these cases [31].